Rafael de Queiroz Garcia

Consecutive laser pulses excitation technique to untangle the dynamics of triplet states in organic molecules

São Carlos
December of 2020

Rafael de Queiroz Garcia

Consecutive laser pulses excitation technique to untangle the dynamics of triplet states in organic molecules

Undergraduate thesis presented to the Physics Undergraduate Program of the São Carlos Physics Institute (IFSC) from University of São Paulo (USP), to obtain the title of Bachelor in Physics.

Advisor: Prof. Dr. Leonardo De Boni – IFSC-USP

São Carlos
December of 2020

Dedicated to my caring family and friends.

To those present from beginning to the end.

To whom, as I expect this seedling to bloom,

holds any fruitful future of my work on their hands.

"Matéria estranha, sempre, ao máximo
se aferra
Ao que já alcançou o pensamento
humano;"

Johan Wolfgang Goethe. Fausto -
Primeira Parte. Translated by Jenny
Klabin Segall

Abstract

This work has the goal of demonstrating a novel photophysical technique able to accurately measure the intersystem crossing rate and efficiency in organic molecules with nonradiative triplet states. The technique was called Consecutive Laser Pulses Excitation, and it measures the fluorescent emission of an ensemble of molecules consecutively excited by distinct laser pulses equally spaced in time. All desired information of the triplet state is indirectly determined via the fluorescence emission, which will suffer quenching depending on the magnitude of the intersystem crossing efficiency. For the calibration of the technique, Rhodamine B and two different porphyrins were used. These are new porphyrins, which had still unknown photophysical parameters. So, an extensive optical characterization was also made for these molecules.

Keywords: Triplet quantum yield. Laser spectroscopy. Time-resolved fluorescence

Resumo

Este trabalho tem como objetivo propor uma nova técnica fotofísica que possui a capacidade de medir acuradamente taxas e eficiências quânticas de cruzamento intersistemas em moléculas orgânicas com estados tripletos não radiativos. A técnica foi denominada Consecutive Laser Pulses Excitation (Excitação com Pulsos Laser Consecutivos) e consiste em medir a emissão de fluorescência de um *ensemble* de moléculas excitadas consecutivamente por diferentes pulsos *laser* igualmente separados temporalmente. Toda a informação desejada sobre os estados tripletos é obtida indiretamente pela emissão de fluorescência, a qual sofrerá uma diminuição a depender da magnitude da eficiência quântica de tripletização dos compostos. Para calibrar a nova técnica, Rodamina B e duas porfirinas diferentes foram utilizadas. Essas porfirinas, sendo ainda novas na literatura fotofísica, ainda não tinham parâmetros fotofísicos importante conhecidos. Sendo assim, além da caracterização do estado tripleto, uma caracterização mais abrangente também foi feita para essas moléculas.

Palavras-chave: Eficiência quântica de tripletização. Espectroscopia a laser. Fluorescência resolvida no tempo

Contents

1   Introduction to Photophysics

The study of the optical properties of organic molecules is necessary to an ever-growing range of applications and technological frontiers. Such are, e.g., the broader employment of OLEDs (Organic Light-Emitting Diodes) in everyday technology (1), development of new lasing media (2), or even detailed inquiries in the microscale with fluorescent probes (3). This is so a necessity, because the knowledge of the photophysical properties allows one to assess objective strategies for trialing and production of new materials for all the latter applications. That is, reliable photophysical studies point out what a molecule is best suited for and provide pathways for successful applications. Furthermore, new applications always rise from novel photophysical phenomena, and hence the field maintains a continuous pertinence.

Beyond its applications, photophysics consists of the study of light absorption and emission by matter, i.e., the light-matter interaction possibilities. Absorption processes occur when molecules in their ground state are excited by light, absorbing its energy and changing their electronic orbital configuration, i.e., executing an electronic transition (4). This process takes place in a time close to the order of magnitude of the period of oscillation of the incident light (tipically $10^{-15}s$). In some conditions, molecules already in an excited state may also absorb light, and this will be discussed later in section 3.3.2.

After excitations, relaxation processes start to take place and may take much more time to finally come to end, from hundreds of fs up to hours. What occurs depends greatly on the energy levels and orbital configurations of the molecule, which may favour radiative or non-radiative decay, or may even allow change in the multiplicity of the state when strong spin-orbit coupling is present, the so called *intersystem crossing*. In this way, a transition may happen between a singlet and a triplet configuration which was in principle forbidden. Spontaneous and stimulated emission can be both responsible for radiative processes in molecules, and vibrational relaxations by energy transfer to the surrounding medium are accounted in the non-radiative processes of relaxation (5).

The variability of the described processes require the use of distinct photophysical techniques in order to deal with the different orders of magnitude and the nature of the involved physical quantities. The main goal of this work was to develop a new technique, which will be called Consecutive Laser Pulses Excitation technique (CLPE). It is able to measure the *triplet quantum yield* and *intersystem*

crossing time of fluorescent organic molecules in solution. There are still few techniques able to measure these quantities, some of which are still very unprecise. So, this work has fully developed this new experimental approach, and also tested it in new samples, with previously unknown photophysical quantities. Not only both referred parameters were measured, but a more complete optical characterization was also done for these molecules, requiring other already established techniques, which will be followingly described along with CLPE.

2 Materials and Methods

2.1 Porphyrins

The new spectroscopic technique set up in this work is able to measure the intersystem crossing time τ_{isc} of molecules in solution. This measurement is specially necessary in the characterization of molecules of the porphyrin class. Thus, two porphyrins with unknown τ_{isc} values were chosen to compose this work. Porphyrins are a group of tetrapyrrolic macrocyclic molecules, which have an extensive history of applications as photosensitizers (PS) (6), and continue to be studied also for catalysis, photocatalysis and even molecular machine applications (7). Presently, there is a great interest in further exploring porphyrins with distinct functional groups and metal complexes, thus pursuing the betterment of a set of properties, e.g., enhanced production of one type of reactive oxygen in PDT, biospecificity in cancer PDT or a simple increase in singlet to triplet conversion, i.e., enhanced intersystem crossing τ_{isc} (6).
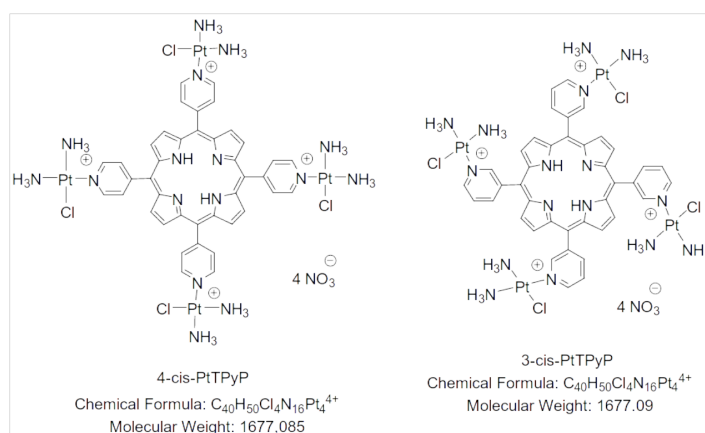
Figure 1: Chemical structure of the two molecules treated in this work.
Source: By the author

The two porhpyrins used in this work, namely 3-cis-PtTPyP and 4-cis-PtTPyP (figure 1), were synthesized in Universidade Federal de Santa Maria (UFSM) in Bioinorganics and Porphyrinic Materials Laboratory (LBMP). Two different solvents were chosen for the photophysical studies. One of which was pure Dimethyl Sulfoxide (DMSO), and the second was a 50/50 volume mixture of distilled water and DMSO. The molecules dissolve fairly better in pure DMSO in comparison to the H_2O/DMSO mixture, and molecular aggregation is avoided for concentrations under 10^{-4} M.

For one of these porphyrins, the generation of singlet oxygen by optical excitation was already demonstrated (8). This strongly indicates the existence of a triplet state on the molecules. However, there is still no study on some of the photophysical properties of these two compounds, and more specifically of the triplet state. So, this work is going to provide a valuable characterization, including fluorescence quantum yields, fluorescence lifetimes and intersystem crossing times τ_{isc} for these two molecules. For achieving this, the physical processes and the relevant timescales should be better understood.

2.2   Photophysical modelling of porphyrins in the nanoseconds regime

Typically, porphyrins can be described by a simplified Jablonsky diagram, depicted in figure 2, which omits vibrational energy levels. The ground state of porphyrins is typically a singlet configuration (S_0), which can be excited to the first excited state (S_1) and also to higher energy states, which are generically referred as S_n. The diagram is built to depict only the $S_0 \not\!/ S_1$ excitation. However, transitions to higher energy levels effectively reproduce the same situation because, after excitation, the tendency of porphyrins is to decay in the form $S_n \not\!/ S_1$ by ultrafast internal conversion processes, the entire relaxation time being lower than 500 fs (9). So, in the timescale of a few picoseconds after excitation, the excited population is mostly in S_1 and few molecules have decayed to S_0, thus explaining why most porphyrinic systems can be modeled as in figure 2.
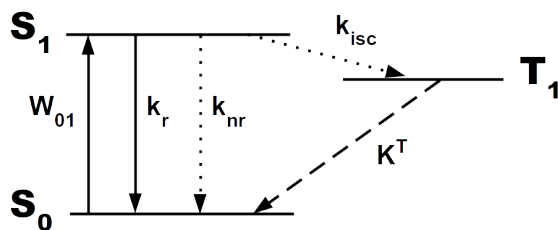
Figure 2: Typical simplified Jablonski diagram for porphyrins excited with the wavelength of the $S_0 \not\!/ S_1$ transition. The solid arrows represent radiative emission (k_r) and absorption (W_{01}) rates, whereas dotted arrows represent non-radiative rates (k_{isc}, k_{nr}). The dashed line represents the decay rate K^T from the triplet state, which is almost totally non-radiative.

Source: By the author

From the Jablonski diagram, it is easy to see what are the possible transitions between energy levels and their respective rates. The absorption rate of the $S_0 \not\!/ S_1$ transition is W_{01}, and the other rates are all from relaxations of radiative nature (k_r) or non-radiative nature, i.e., internal conversion followed by vibronic relaxation (k_{nr} and K^T) and intersystem crossing (k_{isc}). All the rate quantities can be reexpressed as lifetimes of the respective processes, following $\tau = \frac{1}{k}$. Two very important

quantities are $\tau_F = (k_{total})^{-1} = (k_r + k_{nr} + k_{isc})^{-1} = (\frac{1}{r} + \frac{1}{nr} + \frac{1}{isc})^{-1}$ and $\tau_T = (K^T)^{-1}$. Now, although transitions between states of different multiplicities are in principle forbidden, the spin-orbit coupling in porphyrins will loosen this selection rule, and eventually k_{isc} may be even greater than k_r or k_{nr}, which then creates considerable population in the T_1 state. What also happens typically is that $\tau_T \gg \tau_F$, because $\tau_T > 10\,\mu s$ and τ_F is of the order of ns, so it is possible to maintain the population on the T_1 level for a time proportional to τ_T, whereas the population on the S_1 state vanishes some nanoseconds after excitation. With both considerations, about what happens in ultrafast timescales and longer timescales, it is possible to write effective rate equations for the system in the nanoseconds regime:

$$\frac{\mathrm{d}n_0(t)}{\mathrm{d}t} = -n_0(t)W_{01} + \frac{n_1(t)}{\tau_F} - \frac{n_1(t)}{\tau_{isc}} \tag{1}$$

$$\frac{\mathrm{d}n_1(t)}{\mathrm{d}t} = +n_0(t)W_{01} - \frac{n_1(t)}{\tau_F} \tag{2}$$

$$\frac{\mathrm{d}n_T(t)}{\mathrm{d}t} = \frac{n_1(t)}{\tau_{isc}} \tag{3}$$

In which n_0, n_1 and n_T are the fractional populations of S_0, S_1 and T_1 respectively in an ensemble of molecules, i.e., $n_0 + n_1 + n_T = 1$. In equation 1, $\frac{n_1(t)}{F} - \frac{n_1(t)}{isc} = n_1(t)(\frac{1}{r} + \frac{1}{nr})$, which is expected, because in nanosecond timescale, only k_r and k_{nr} contribute to repopulation of the ground state. The same reason explains why there is no negative rate term on equation 3.

Now, the reason why this mechanism of building a population in the triplet state is important, is because porphyrins may collide with other molecules and then transfer their energy to them. This has a high probability of happening till time τ_T, and that is one of the main interests in applications. Energy transfer to an Oxygen molecule will create a reactive oxygen, which may then help destroy tumorous cells in PDT applications. So, it shall now be discussed how the relevant photophysical quantities will be obtained for the first time for the molecules in this work. This is always done in a constructive manner, in a way that each experimental technique will provide new information that will allow the next technique to be correctly applied.

2.3 Linear optical characterization

2.3.1 Absorption spectra and Fluorescence quantum yield

The first optical characterization on both molecules in the two solvents was obtained with linear absorption spectroscopy, using Shimadzu UV-1800 spectrophotometer. This allows one to obtain information about the absorption bands and, therefore, the energy levels of the molecule. Furthermore,

this equipment is important to calibrate solutions to equal absorbance values for use in fluorescence measurements. In these measurements, the objective is to obtain the *fluorescence quantum yield* η_F, which states how much of the light energy absorbed by a molecule is reemitted as radiation specifically in the $S_1 \to S_0$ relaxation (see fig. 2). This quantity can be clearly related to the relaxation rates, being defined as $\eta_F = \frac{k_r}{k_{total}}$, along with other quantities $\eta_{IC} = \frac{k_{nr}}{k_{total}}$ and $\eta_T = \frac{k_{isc}}{k_{total}}$, which are the *internal conversion yield* and *triplet quantum yield*, respectively.

To measure η_F, a Hitachi F7000 fluorimeter was used. The used procedure, frequently referred as Brouwer's method (10), uses a sample with an already determined η_F. This was the case of a protoporphyrin IX molecule (PPIX), which has $\eta_F^{PPIX} = 8.5\%$ in pure DMSO solution (9), and which became a standard in these linear optical characterization procedures. As it is not the main scope of this work, the details about the method are left to the appendix A. The results for η_F are available in table 1 and will be important, principally, to sort out the value of η_{IC}, because $\eta_{IC} = 1 - \eta_F - \eta_T$, and η_T will be measured with the CLPE technique. So, η_F helps in fully characterizing the radiative processes and helps measuring indirectly the non-radiative ones.

2.3.2 Time-resolved fluorescence measurements (TRF)

Another very important photophysical parameter is the fluorescence lifetime τ_F. As the CLPE technique monitors consecutive fluorescence decays, the determination of τ_F is a necessary prior step. To measure it, a setup like in figure 3 was used. It consists of a *Light Conversion Pharos* laser system, used with 1 kHz repetition rate, and 220 fs pulse duration. The excitation wavelength used was 515 nm, coincident with the $S_0 \to S_1$ absorption band of the porphyrins. A simple set of mirrors and a focusing lens can be used to direct the laser beam to the sample, and then an optical fiber, placed perpendicularly to the beam, gathers the fluorescence light and redirects it to a photodetector of rise and fall time of 700 ps. A filter is placed between the end of the fiber and the detector to avoid the detection of excessive scattered laser radiation. An 1GHz bandwidth oscilloscope then registers the signal of the detector.
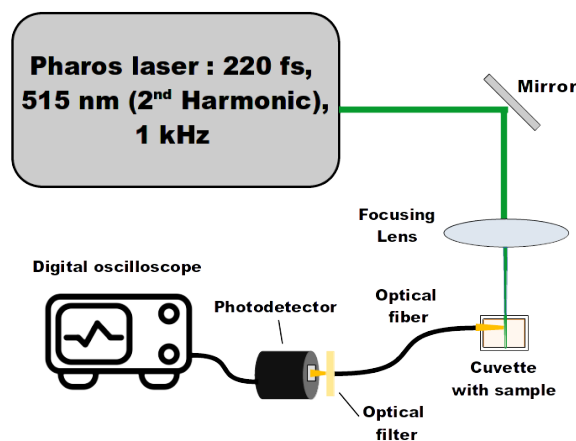
14

Figure 3: Experimental setup for performing time-resolved fluorescence.
Source: By the author

Porphyrins have fluorescence lifetimes of the order of nanoseconds, which may be very close to the time resolution of commercially available photodetectors. What happens then, is that the expected fluorescence signal will experience distortions in time which are intrinsic from the equipment used. So, in order to appropriately measure a fluorescence decay curve, it is necessary to consider the *Instrument Response Function* (IRF). A possible way of measuring the IRF is to simply use a scatterer of laser light in the entrance of the optical fiber, which will stimulate the detector in a timescale way inferior to its time resolution (220 fs $\ll$ 700 ps), i.e., it will act as an almost instantaneous stimulation. Then, a model $I_F(t)$ should be chosen and convoluted with the IRF to fit the fluorescence signal $S_F(t)$. This convolution operation is normally written as $S_F(t) = (I_F * IRF)(t) = \int_{-\infty}^{\infty} I_F(\tau)IRF(t - \tau)d\tau$, and for the porphyrins, only one decay time for the fluorescence is expected. So, I_F can be modelled as $I_F(t) = e^{-t/\tau_F} + r e^{-t/\tau_e}$, which leaves the fitting algorithm with three free parameters. The second exponential has always $\tau_e \ll \tau_F$ and a relative amplitude of r. It is a normal procedure in convolution fitting to introduce this additional exponential in the model to account for fast-occurring processes, one of which is the scattering of laser light. It always occurs prior to fluorescence emission and it may correspond to a high percentage of the initial amplitude of the fluorescence curve. The fitting procedure was made using a non-linear least squares algorithm, which was implemented in the *python* programming language. This TRF convolution method was already calibrated in the used detector with organic molecules of known τ_F values, such as Rhodamine 6G. Here, to demonstrate the calibration, the TRF for a Rhodamine B sample was made.

Furthermore, there is a feature in the fitting process in TRF for which higher excitation intensities tend to diminish the τ_F and τ_e values, increasing r. This supposedly happens because, for higher intensities, the amount of scattered laser radiation also increases. At some point, the optical filter

cannot sufficiently attenuate the scattered radiation. It follows that the τ_e exponential may not be sufficient to incorporate all the rapidly occurring phenomena, incurring in a change in τ_F too. The typical procedure then to measure reliable τ_F values was to maximize the fluorescence light gathering and to measure at the lowest excitation intensities as possible. The so far discussed and experimentally measured parameters are of paramount importance to determine the triplet state population transfer. More than that, the τ_F value is a necessary input parameter in the modeling and interpretation of the results of the CLPE technique, which will be now described.

2.4 Triplet state determination: Consecutive Laser Pulses Excitation Technique (CLPE)

In this work, a new spectroscopic technique based on consecutive time-resolved fluorescence signals was developed to determine the population transferred to nonradiative triplet states. The Consecutive Laser Pulses Excitation technique (CLPE) is built with the apparatus displayed on figure 4. It is based on the time-monitoring of the fluorescence of a sample subject to consecutive excitations driven by fs-laser pulses. On the nanoseconds timescale, each excitation can promote part of the molecules to a triplet state, hence quenching the fluorescence emission of subsequent excitations. All the characteristics of the triplet state are then measured indirectly using the fluorescence signal and, in the case of this work, exploring equations (1) to (3).

The technique relies on the same laser system from the setup in section 2.3.2, but it is now operated in a lower repetition rate, of 100 Hz, willing to avoid accumulative thermal effects in the sample. In order to generate consecutive pulses for excitation, the laser beam is directed to a ring cavity. In this configuration, the beam is first incident in an approximately 50/50 reflection/transmission beamsplitter. The reflected beam is the first to excite the sample, while the transmitted beam travels around the ring cavity in a controllable $\top$ time. This cavity has highly reflective mirrors (R > 99%) but which still cause some energy loss. After one revolution, the beam is again partially transmitted and reflected, which splits the beam in an again cavity-traveling and in another excitation beam. The cavity output pulse is then properly aligned to always provide excitation in the same spatial region of the sample, exciting also always the same molecular population. The interpulse time interval is always $\top$, and the consecutive pulses are periodically extracted from the cavity until their complete extinction, which happens, typically, after 4 cycles. Also, T was chosen as 9.5 ns, a value higher than the fluorescence lifetime of the used samples. The cavity is built with aluminum mirrors, which

allows one to use the technique in any wavelength available in the tunable laser system, i.e., allows UV-Vis-IR excitation.
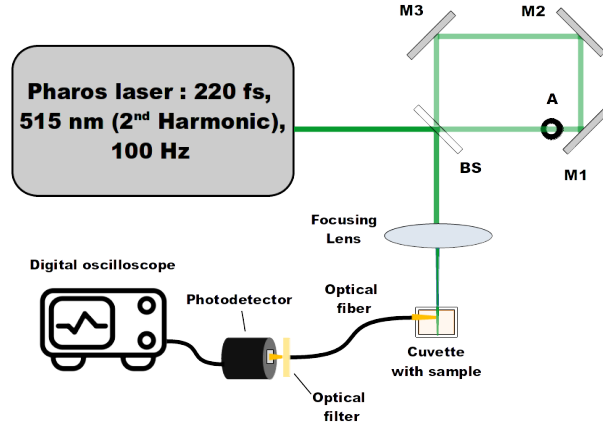

Figure 4: Experimental setup for the CLPE technique. In addition to the setup shown in figure 3, a ring cavity was built to generate the consecutive excitations. It is composed of a beamsplitter (BS), three aluminum mirrors (Mi), and an aperture (A) to select the correct reflection from the beamsplitter. The laser is now set to a 100 Hz repetition rate.

2.4.1 Physical modelling of CLPE for porphyrin triplet state dynamics

Due to the described experimental conditions and sample parameters, the rate equations that describe the system (eqs. (1) to (3)) can be simplified, allowing for a very straightforward solution. It is possible to consider each excitation occurring instantly because of the ultrafast laser pulses, and then the equations can be piece-wise solved in the interpulse intervals T. Equations 1 and 2 can be represented in the $(j-1)\,T \leq t < (j)\,T$ intervals, in which $j = 1, 2, 3, ...$ indicates the jth consecutive excitation.

$$n_0(t)_j = n_0(T)_{j-1} e^{-\frac{F_j}{h\nu}}$$
$$+ [n_1(T)_{j-1} + n_0(T)_{j-1}(1 - e^{-\frac{F_j}{h\nu}})](1 - \frac{\tau_F}{\tau_{isc}})(1 - e^{-t=F}) \qquad (4)$$

$$n_1(t)_j = [n_1(T)_{j-1} + n_0(T)_{j-1}(1 - e^{-\frac{F_j}{h\nu}})] e^{-t=F} \qquad (5)$$
$$n_1(0)_j\, e^{-t=F}$$

In these equations, the time-integrated absorption rate W_{01} is written as $\sigma_{01}\frac{F_j}{h}$, in which σ_{01} and $h\nu$ are the absorption cross section and energy of the transition, respectively. F_j is the time-integrated fluency of the jth pulse. A more complete model would also have to consider the spatial integration of the population. According to the Beer-Lambert law $F_j(z) = F_j^0 exp(-C n_0(T)_{j-1}\sigma_{01} z)$. That means F_j is exponentially attenuated while propagating through a distance z in a cuvette with por-

phyrins at a C concentration. The attenuation depends on $n_0(\tau)_{j-1}$ because the *total* population in the ground state before an excitation is $C\,n_0(\tau)_{j-1}$. However, the necessity of spatial integration is avoided using low solution concentrations , for which $C\sigma\,l \ll 1$, with $l = \ell_2 - \ell_1 \approx 1mm$ being the typical cuvette length from which the optical fiber gathers light. In the equation, ℓ_1 and ℓ_2 are the lengths measured from the face of the cuvette in which the beam is incident. Alternatively, using high F_j fluencies will also avoid the use of spatial integration, in behalf of $\frac{1}{\ell_2 - \ell_1}\int_{\ell_1}^{\ell_2} e^{-\frac{F_j(z)}{h\nu}}dz$ becoming a small value, meaning almost total population transfer from n_0 to n_1. The latter is a frequently achieved condition in the used experimental setup and very high population transfers were indeed verified.

To provide a time-resolved analysis of the fluorescence, equation (5) will be the basis of the model function $I_F(t)$, which now requires new hypotheses. Now, it will be necessary to consider $I_F(t)_j$ also in the $(j-1)\tau \le t < (j)\tau$ intervals. The fluorescence intensity is proportional to the total population in the n_1 state. At a time τ after excitation, the remaining population is $n_1(\tau_{j-1})$ and the incoming excitation will produce an increment $\Delta n_1(0)_j = n_0(\tau)_{j-1}(1 - e^{-\frac{F_j}{h\nu}})$ in the population. One should expect that, following the reasoning of section 2.3.2, the increment in fluorescence would be $\Delta n_1(0)_j\, I_F(t) = \Delta n_1(0)_j[e^{-t/\tau_F} + r\,e^{-t/\tau_e}]$ and thus the model function should be written, modifying equation (5), as

$$I_F(t)_j \propto \Delta n_1(0)_j\, e^{-t/\tau_F} + \Delta n_1(0)_j\, r\, e^{-t/\tau_e} \tag{6}$$

However, the assumption that the pre-exponential factor r is the same throughout the consecutive pulses is questionable, because r codifies the information about the scattered light, although in a very non-linear manner. As the relative intensity of scattering and fluorescence emission changes between consecutive excitations, r may also change. If this indeed happens, this will affect the determination of τ_{isc}. So, in section 3.3.1, an experimental motivation for this assumption is presented. For now, it is important to note that τ_F was already previously determined in the single-excitation time-resolved fluorescence, as well as the IRF. However, r and τ_e are redetermined for each different CLPE condition. This is done performing the same fitting procedure as in section 2.3.2 but in a timespan between the first excitation and some ps before the second excitation. This allows one to account for different magnitudes of fast phenomena that may occur at higher laser powers. Possibly, one can even extend the model of equation (6) with an extra exponential term $\propto \Delta n_1(0)_j\, r_2\, e^{-t/\tau_{e2}}$, and this will be further explored in section 3.3.3.

The information about τ_{isc}, the quantity measured by this technique, is located in $\Delta n_1(0)_j$. If one

also looks closely, τ_{isc} only appears in eqs. (4) to (5) in the form of a ratio. So, if it is left as a free-parameter, what is really determined by the model is $\phi_T = \frac{\tau_F}{\tau_{isc}}$, the triplet quantum yield. Using the obtained τ_F value and propagating the error, one can then obtain the τ_{isc}. What still lacks being discussed for the determination of $n_1(0)_j$ is the measurement of the relative fluencies F_j. This is done with the same scatterer used in measuring the IRF, which now scatters the consecutive pulses to the detector, and their peak intensities f_j, as measured in the oscilloscope, are used as an intensity parameter. This, of course, requires the linearity of the detector.

Further simplifications can be done in the model. As even more would need to be assumed about the focalization and attenuation of the laser beam in the sample, what is done is to define a proportionality constant α, stating that $F_j = \alpha f_j$. This then yields $\sigma \frac{F_j}{\hbar} = \sigma_a f_j$, with $\sigma_a = \sigma \frac{\alpha}{\hbar}$. And hence, σ_a is introduced as a free parameter in the fitting from equation (5). This linearity condition between F_j and f_j is not satisfied if, again, the effect of spatial integration is considered. Even so, this free parameter is not discarded as an unuseful artifact, because it is independent of the other free parameter of the model τ_{isc}, which is the one that needs to be obtained with certainty. Additionally, σ_a becomes an effective absorption cross section for the solution, for which one can define the excitation parameter $\sigma_a f_1$, that accounts for the effective population transfer promoted by the first excitation, because $n_1(0)_1 = (1 - e^{-\sigma_a f_1})$.

With all of this considered, the experiments with the CLPE technique then consisted on varying the intensity of the laser, i.e., changing f_j, and monitoring the fitted τ_{isc} values. In principle, τ_{isc} should not depend on the intensity. However, as the optical fiber collects a spacial average of the fluorescence, only for high fluencies one is able to see the stabilization of the τ_{isc} values (figure 5). It is important to progressively increase the intensity to see if this behavior is always present an then to attribute the correct value of τ_{isc} to measurements in this regime. On the other hand, the fluency cannot be increased indefinitely, because thermal effects soon tend to take place, which causes thermal lensing, changing the relative intensity of the fluorescence peaks, and also causing thermal degradation of the sample. This is then the main trade-off in the technique, one between populational effects at low fluencies, and thermal effects at high ones.

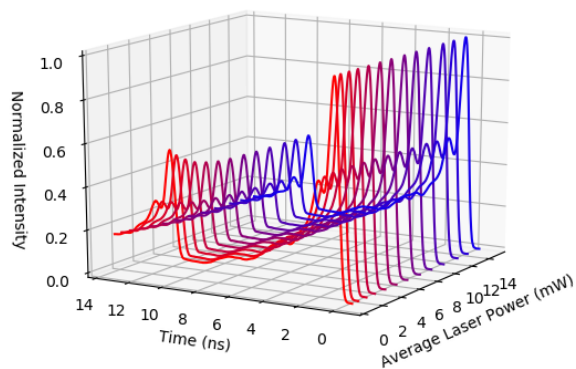CLPE fluorescence signals as a function of laser power
for 3-cis-PtPyP in DMSO

Figure 5: Normalized fluorescence signals for different laser powers are here depicted. One can see a decrease in the fluorescence intensity and a stabilization behavior for increasing laser power for the second peak of fluorescence. This is expected to appear if the first pulse is able to fully excite the molecules in the spatial region from which the fluorescence signal is gathered. This phenomenon also stabilizes the value of τ_{isc}.

Source: By the author

3 Results and Discussions

3.1 Absorption and Fluorescence spectra

The four absorption and fluorescence spectra studied are shown in figure 11, in Appendix A. The porphyrins all had a peak molar absorptivity ϵ of around $2.0 \ 10^5 \ \ell \ cm^{-1} mol^{-1}$ on the 420 nm $S_0 \ / \ S_2$ band, and the bands found between 490 to 600 nm correspond to lower ϵ Q bands, all of which represent $S_0 \ / \ S_1$ transitions and are all expected in porphyrin spectra (11). The band centered in 515 nm has molar absorptivities between $1.0 \ 10^4$ and $2.0 \ 10^4 \ \ell \ cm^{-1} mol^{-1}$ and coincides with the laser wavelength used for TRF and CLPE. For the fluorescence spectra, it was possible to see reduction in fluorescence intensity, and thus in $_F$, for both porhpyrins in the 50/50 DMSO/H_2O solution, in comparison to pure DMSO. The results are displayed in table 1. One should note the very low values of $_F$, i.e., below 1%.

3.2 Time-resolved fluorescence

The time-resolved fluorescence was measured with 5 different laser intensities for the two molecules in the two solvents and also for Rhodamine B in ethanol. As already stated, the measurements were all performed in low laser intensities and maximizing the fluorescence gathering from the sample, in order to avoid excessive transient response in the fluorescence curve. Three examples of fitted curves are presented in figure 12 in Appendix B. In this kind of fluorescence measurements, the attributed error is of 10%. The Rhodamine B sample yielded $\tau_F = 2.8 \ 0.3 \ ns$, which is in agreement with the literature (12). The samples dissolved in DMSO/H2O showed lower lifetimes than the ones dissolved in DMSO. For the 4-cisPtTPyP molecule, the $\tau_F = 0.61 \ 0.06 \ ns$ value is on the limit of resolution of the equipment (0.7 ns), so τ_F might be even shorter. The other obtained τ_F values range between $7.6 \ ns$ and $2.6 \ ns$ and are displayed in table 1.

Table 1: The so far determined photophysical quantities are here presented. The 3-cis-PtTPyP and 4-cis-PtTPyP molecules were labeled as 3-cis and 4-cis for better readability. After measuring ϕ_F and τ_F, with 5% and 10% precision respectively, it was possible to derive some other photophysical quantities. However, to distinguish between k_{nr} and k_{isc}, the CLPE technique will be needed.

Porphyrin /Solvent	ϕ_F (%)	τ_F (ns)	k_r ($10^7 s^{-1}$)	τ_r (ns)	$k_{nr} + k_{isc}$ ($10^7 s^{-1}$)
3-cis / DMSO	0.82	7.6	0.11	900	13
3-cis / DMSO/H2O	0.07	2.6	0.03	3800	38
4-cis / DMSO	0.67	6.8	0.10	1000	15
4-cis / DMSO/H2O	0.07	0.61	0.11	900	160

Source: By the author

3.3 Determination of the intersystem crossing time and triplet quantum yield of porphyrins

3.3.1 Validation of the model for CLPE

As discussed in section 2.4.1, each excitation also brings scattered laser light into the detector, and this contribution may affect the peak fluorescence intensity following after the excitation, which in turn influences the τ_{isc} determination. So, to test the validity of the model in equation (6), which will be now called M(a) model, the Rhodamine B molecule was used. It was chosen because the intersystem crossing time is very long ($> 1\ \mu s$) compared to the τ_F measured in the last section (13). So, the population transferred to T_1 (figure 2) is negligible. This would allow one to rule out the τ_{isc} as a free fitting parameter, thus leaving only σ_a. This is, of course, not sufficient to prove equation (6) may be true, but if the temporal profile can be reproduced using this hypothesis, it should endorse that the τ_{isc} measurements are not affected by significant variation of the r parameter. The result of the applied CLPE model is depicted in figure 6.
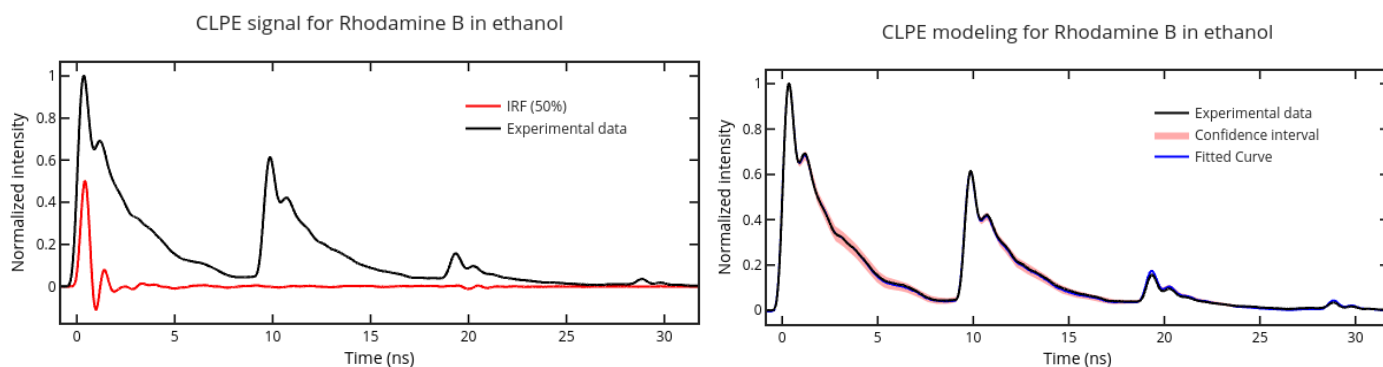

Figure 6: On the left, the experimental data show the fluorescence decay of consecutive excitations of Rhodamine B in ethanol. On the right, the fitted curve is a test of model M(a), again considering a τ_F error of 10% for the confidence interval.

Source: By the author

The experiment was conducted in 5 different laser powers in increasing order (from 0.3 to 3 mW), with sample degradation occurring for a power greater than 2 mW. No significant fluorescence quenching was observed along this process, which confirms the consistency of the CLPE technique for samples with no significant T_1 population. As it can be seen, the fitted curve adheres very well to the experimental data, yielding also a very low Residual Standard Error.

3.3.2 CLPE for 3-cis-PtTPyP and 4-cis-PtTPyP molecules: intersystem crossing quantities determination

After validating the analytical method with an organic sample with no significant population in triplet state, the CLPE technique was used to obtain the triplet quantum yield and intersystem crossing time of the new porphyrins. In the experiment, increasing equally spaced laser powers, ranging between 0.7 mW and 15 mW, were used. This range was chosen because, although higher powers led to thermal effects and sample degradation, only for powers around 10 mW, stabilization of τ occurred. This stabilization, as already discussed and shown in figure 5, being a consequence of the spatial averaging of the fluorescence signal. At least 11 different CLPE curves were fit for each sample by the model M(a), so only the stabilized condition is going to be depicted in this section, being the other conditions such as the ones represented in figure 5. Beginning with the results for 3-cis-PtTPyP and 4-cis-PtTPyP in the DMSO solution, the fitting for the CLPE technique is shown in figure 7. For clarity, the pure signal with the IRF was represented in a different graph (7.a and 7.c) from the fitted model (7.b and 7.d), because there are regions with a lot of overlap, which is, of course, an evidence that the model greatly captures the behavior of the time-resolved technique.
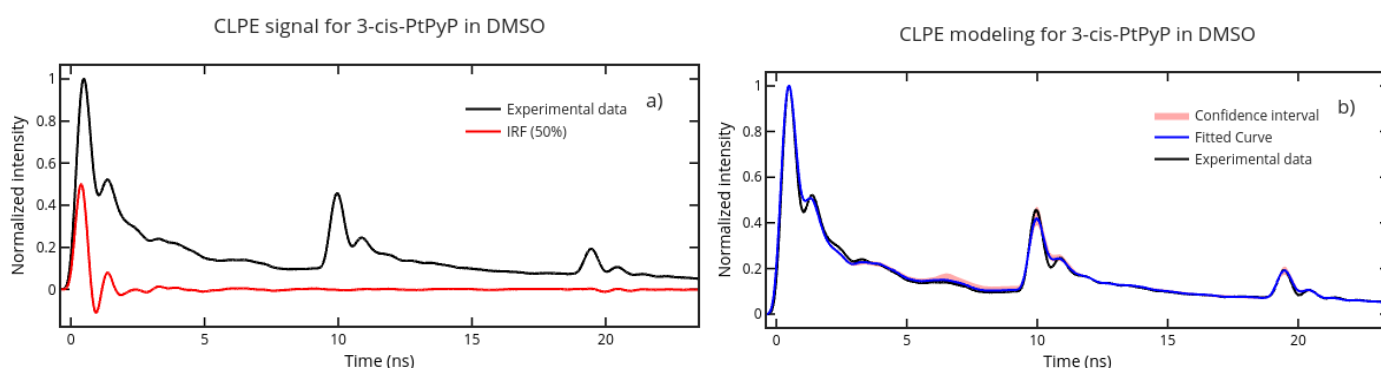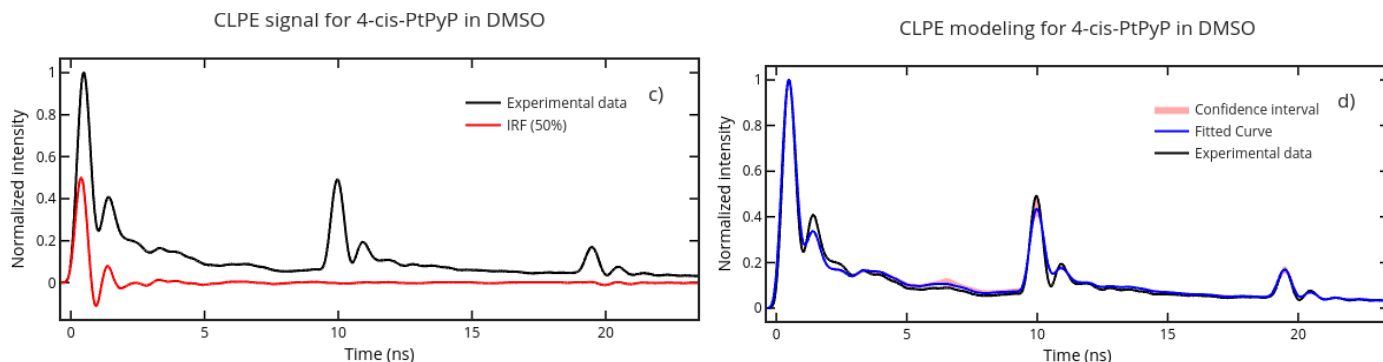
Continuation

Figure 7: The two molecules dissolved in DMSO had their CLPE signals modeled by equation (6). The result is shown in the upper two graphs for 3-cis-PtTPyP (a) and b)) and in the bottom for 4-cis-PtTPyP (c) and d)). One can see the confidence intervals, which consider an error of 10% in τ_F, are particularly wider at the peak of excitations.

Source: By the author

For the 4-cis-PtTPyP in DMSO sample, it is possible to see little behavior deviations at short times after excitation (< 2 ns). One may ask if the lack of a better overlap between the model and the signal in this range affects the measurement of τ_{isc}. What will be shown in section 3.3.3 with a different model M(b), is that the current M(a), is sufficiently robust to these variations, producing a reliable result. Furthermore, the differences between the signal and the model immediately at the excitation peaks, which are the critical regions for the fitting of the curve, are explained by the 10% error in τ_F. This is important to know because it gives the magnitude of what is really being measured when the model fits the peaks at a specific height. If the confidence interval does not overlap the signal at the peak, the measured value for τ_{isc} should have a greater error incorporated. Fortunately, this was not the case, as the fitting was indeed adequate. To intuitively address what a very high error in the model would mean, some attempts to force the fitting to other τ_{isc} values are shown in Appendix C. Now, the remaining results, for the two molecules in the 50/50 DMSO/H$_2$O solution, are shown in figure 8. An even better agreement for both is demonstrated, and the time-resolved signal is reproduced in the different time domains of the decay curves.
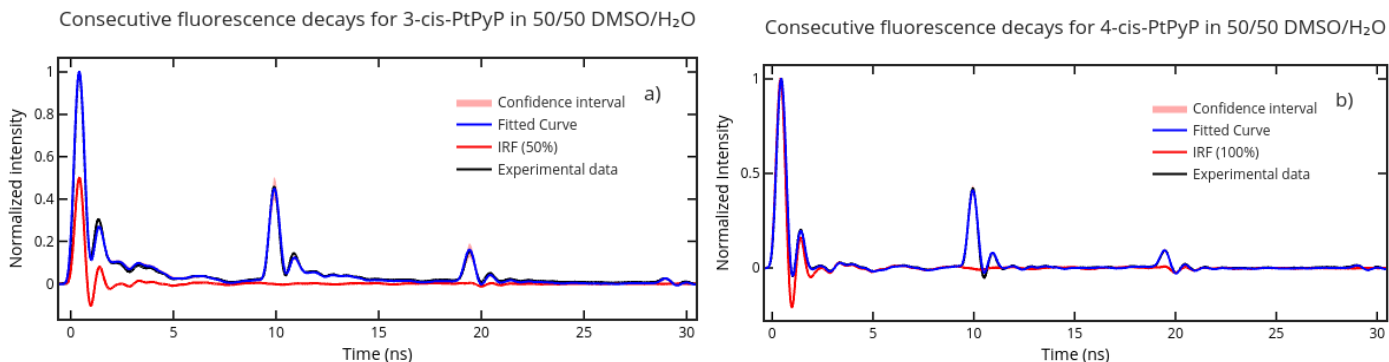
24

Figure 8: Two CLPE signals driven with a laser power of around 10 mW. In a), the situation for 3-cis-PTtPyP is represented and one can see the confidence intervals are particularly greater at the peak of excitations. In b), the CLPE for 4-cis-PtTPyP is shown. Although the fluorescence signal is just a tiny "deformation" of the IRF, it was possible to observe the quenching of fluorescence.

Source: By the author

Now, the free parameters from the model obtained at the different intensities will be shown. The τ and $\sigma_a f_1$ values for all samples are presented in figures 9 and 10. What is effectively measured with the modeling is the ratio $\tau = \frac{F}{isc}$. So, for determining τ_{isc} taking into account the τ_F error, one can average the τ values obtained in the saturated powers and then calculate $\tau_{isc} = \frac{F}{\tau}$ with the proper error propagation, taking into the account the 10% error on τ_F. These results are presented in table 2. What should be noted on both τ and $\sigma_a f_1$, are the thermal effects for power values over 9 mW in the DMSO/H_2O samples, which are more noticeable in the abrupt changes in $\sigma_a f_1$. The measurements in this region were not considered in the determination of the final values of τ. It should be clear now, by figure 9, how well-defined this saturation region is. This behavior is always expected to be followed, and is the main feature that guarantees the value of the obtained τ. Now it is important to restate that this determination of the τ values presented was the successfully achieved main goal of this work. The CLPE technique has shown a very good viability for the four samples, allowing one to obtain very useful information about the triplet state.
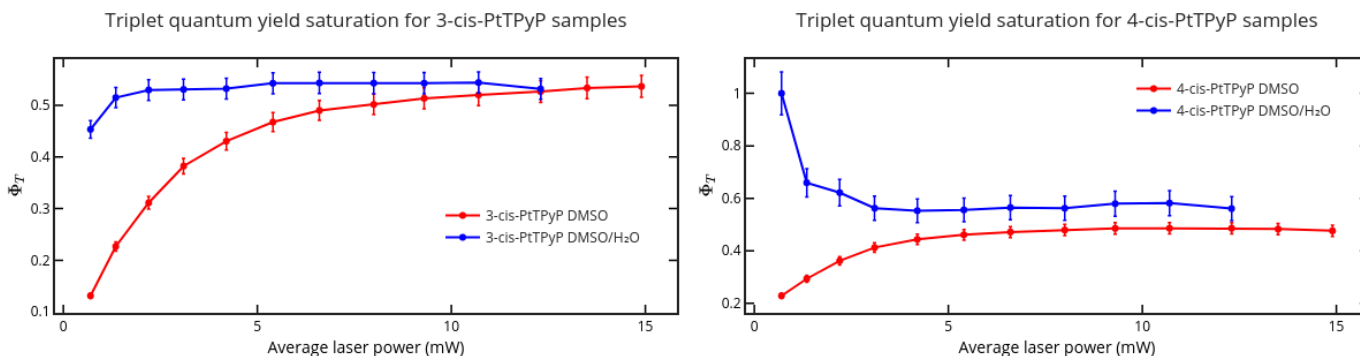

Figure 9: Triplet quantum yield determination as a function of laser power for the four samples. The value for τ obtained in the saturation region is the main experimental result sought by the CLPE technique.

Source: By the author

Moreover, the excitation factor ($\sigma_a f_1$) also suffers a weaker saturation effect as a function of laser power. It is important to note that for $\sigma_a f_1 > 3$, the first pulse excites 95% of the spatially averaged population. As an even greater excitation is achievable for higher laser powers, excited state absorption may occur, and it is possible, in this manner, to saturate the excitation parameter. This happens because excited state absorption uses the irradiation energy not with the purpose of transferring molecules from the ground to an excited state, but further excites molecules that are already going to contribute to the fluorescence intensity. So, the effective excitation parameter accounting for the emitted fluorescence is expected to have a decreased rate of growth with increasing laser power. It is not possible to completely affirm this is actually happening, as the excited state absorption cross section was not measured, but those are often found to be similar to the ground state cross-sections (9).
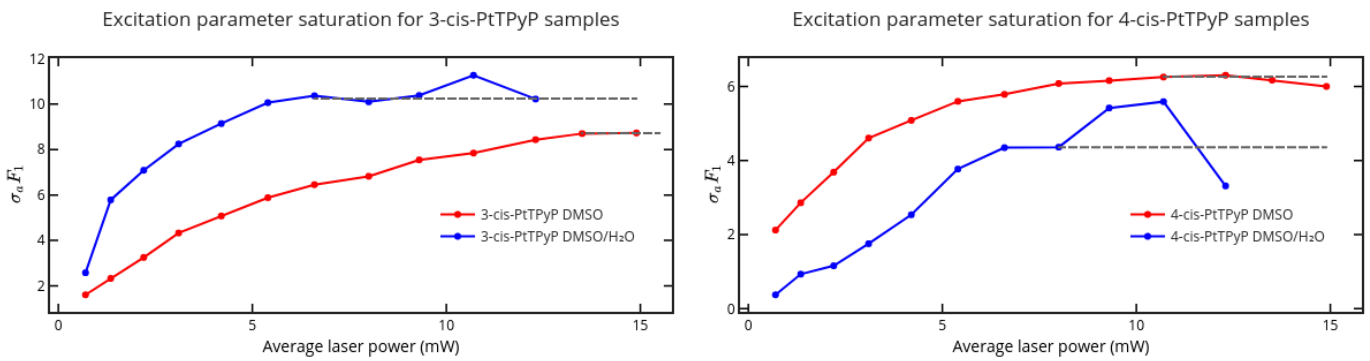

Figure 10: Excitation parameter as a function of laser power for the four samples. It should be noticed that the regions of sudden change in the excitation parameter for high laser powers coincide to when thermal effects begin to occur. A dashed line is then plotted to indicate the expected behavior of the curve if these effects were not present.

Source: By the author

Further considerations on the obtained η_T and τ_{isc} need to be presented. For 4-cis-PtTPyP in DMSO/H$_2$O, there may be a problem in the accuracy caused by the τ_F value, which is in the limit of detection of the equipment, and this error is propagated to the CLPE experiment. Additionally, it is possible to see an increase in η_T for the DMSO/H$_2$O samples. This occurs along with a not necessarily equal decrease in η_F, but it is shown that the overall non-radiative processes are intensified in the DMSO/H$_2$O mixture ($\eta_{IC} + \eta_T = 1 - \eta_F$ is increased). The obtained values for η_T are in the expected order of magnitude for free-base porphyrins (9, 11). Also, the results for M(b) in table 2 will be clarified in the next section.

Table 2: Final results obtained with the CLPE technique. The 3-cis-PtTPyP and 4-cis-PtTPyP were labeled as 3-cis and 4-cis for better readability. M(a) refers to the model in eq. (6), whereas M(b) is explained in section 3.3.3.

	3-cis DMSO		3-cis DMSO/H_2O		4-cis DMSO		4-cis DMSO/H_2O	
Model	M(a)	M(b)	M(a)	M(b)	M(a)	M(b)	M(a)	M(b)
τ (%)	53	50	54	53	48	44	56	56
τ_{isc} (ns)	14 1	15 2	4.9 0.5	5.0 0.5	14 1	15 2	1.1 0.1	1.1 0.1

Source: By the author

3.3.3 Comparison with another model for CLPE

In the CLPE experiment, as the laser power increases, there is also an increase in the amount of scattered laser radiation that arrives in the detector. What one then typically is able to observe is an increasing Residual Standard Error (RSE) for the fitted model. This occurs because of the lack of overlap at the beginning of the fluorescence decay curve, as is observable in figure 7 for 4-cis-PtTPyP. To analyze how this behavior affects the final result of τ, an extra exponential term was proposed to attempt to adequately fit the regions of the curve right after excitation. This is the so called model M(b), for which the results are available in table 2. It consists, as said in section 2.4.1, on adding another fast exponential term $\diagup \quad n_1(0)_j \; r_2 \; e^{t=e2}$ in model M(a). As presented in the table, little difference between the two models is observed if one considers the intrinsic error of 10% in the experiment. One fitting result is shown in figure 14 in Appendix D, along with the RSE obtained for each fitted curve and both models for 4-cis-PtTPyP in DMSO. Although there was a decrease in the RSE values, this did not profoundly change the obtained values, so the preceding model was already sufficiently robust for capturing the essential behavior of the CLPE signal. As M(a) possibly avoids the problem of over-fitting, there is no sufficient motivation to prefer the M(b) model.

4 Conclusion

The Consecutive Laser Pulses Excitation technique was successfully set up and tested throughout this work. The complex considerations about the spatially averaged fluorescence signal were tackled with a sufficiently physical model, which has shown robustness when subject to distinct validations. The measurement of ϕ_T and τ_{isc} are then accounted as trustworthy and the technique will continue to be used for optical characterizations in the Photonics Group from IFSC-USP. The obtained values of ϕ_T ranged between 48% and 56%, whereas the τ_{isc} values ranged between 1 ns and 14 ns. Moreover, not only the triplet state characteristics for both molecules were measured in this study, but also the fluorescence quantum yields and fluorescence lifetimes. This provided an extensive characterization for the porphyrins in both solvents.

References

1 FORREST, S. R. Waiting for Act 2: what lies beyond organic light-emitting diode (OLED) displays for organic electronics? **Nanophotonics**, Berlin, v. 10, n. 1, p. 20200322, 24 Aug. 2020.

2 JIANG, Y.; LIU, Y.-Y.; LIU, X.; LIN, H.; GAO, K.; LAI, W.-Y.; HUANG, W. Organic solid-state lasers: a materials view and future development. **Chemical Society Reviews**, The Royal Society of Chemistry, v. 49, n. 16, p. 5885–5944, 2020.

3 DRUMMEN, G. Fluorescent probes and fluorescence (microscopy) techniques — illuminating biological and biomedical research. **Molecules**, v. 17, n. 12, p. 14067–14090, Nov. 2012.

4 VALEUR B.; BERBERAN-SANTOS, M. . N. Absorption of ultraviolet, visible, and near-infrared radiation. *In:* VALEUR B.; BERBERAN-SANTOS, M. . N. **Molecular fluorescence:** principles and applications. 2nd ed. New York: John Wiley & Sons, Ltd, 2012. chap. 2, p. 31–51.

5 VALEUR B.; BERBERAN-SANTOS, M. . N. Characteristics of fluorescence Emission. *In:* VALEUR B.; BERBERAN-SANTOS, M. . N. **Molecular fluorescence:** principles and applications. 2nd ed. New York: John Wiley & Sons, Ltd, 2012. chap. 2, p. 53–74.

6 ZHANG, J.; JIANG, C.; FIGUEIRÓ LONGO, J. P.; AZEVEDO, R. B.; ZHANG, H.; MUEHLMANN, L. A. An updated overview on the development of new photosensitizers for anticancer photodynamic therapy. **Acta Pharmaceutica Sinica B**, v. 8, n. 2, p. 137–146, 2018.

7 DRAIN, C. M.; VAROTTO, A.; RADIVOJEVIC, I. Self-organized porphyrinic materials. **Chemical Reviews**, v. 109, n. 5, p. 1630–1658, 2009.

8 NAIK, A.; RUBBIANI, R.; GASSER, G.; SPINGLER, B. Visible-light-induced annihilation of tumor cells with platinum–porphyrin conjugates. **Angewandte Chemie International Edition**, v. 53, n. 27, p. 6938–6941, 2014.

9 GOTARDO, F.; COCCA, L. H.; ACUNHA, T. V.; LONGONI, A.; TOLDO, J.; GONÇALVES, P. F.; IGLESIAS, B. A.; DE BONI, L. Investigating the intersystem crossing rate and triplet quantum yield of Protoporphyrin IX by means of pulse train fluorescence technique. **Chemical Physics Letters**, v. 674, p. 48–57, 2017.

10 BROUWER, A. Standards for photoluminescence quantum yield measurements in solution. **Pure Applied Chemistry**, v. 83, n. 12, p. 2213–2228, 2011.

11 SOUZA, T. G. B.; VIVAS, M. G.; MENDONÇA, C. R.; PLUNKETT, S.; FILATOV, M. A.; SENGE, M. O.; DE BONI, L. Studying the intersystem crossing rate and triplet quantum yield of meso-substituted porphyrins by means of pulse train fluorescence technique. **Journal of Porphyrins and Phthalocyanines**, v. 20, 01n04, p. 282–291, 2016.

12 KRISTOFFERSEN, A.; ERGA, S.; HAMRE, B.; FRETTE, Ø. Testing fluorescence lifetime standards using two-photon excitation and time-domain instrumentation: Rhodamine B, Coumarin 6 and Lucifer Yellow. **Journal of Fluorescence**, v. 24, p. 1015–1024, May 2014.

13 WIEDMANN, J.; PENZKOFER, A. Excited-state absorption cross-sections in rhodamine dyes determined after molecular reorientation. **Nuovo Cimento B**, v. 63, p. 459–469, May 1981.

14 KARSTENS, T.; KOBS, K. Rhodamine B and rhodamine 101 as reference substances for fluorescence quantum yield measurements. **The Journal of Physical Chemistry**, v. 84, n. 14, p. 1871–1872, 1980.

Appendix A Absorption spectroscopy and fluorometry

Brouwer's method

This method for obtaining ϕ_F uses measurements of fluorescence emission intensities $F(\lambda)$, integrating them over the appropriate fluorescence emission range $[\lambda_0, \lambda_1]$. It also uses the intensity of light absorbed by the sample in the wavelength of excitation, i.e., $f(\lambda) = 1 - 10^{-A(\lambda)}$, in which $A(\lambda)$ is the wavelength-dependent sample absorbance measured in the spectrophotometer. In principle, the ratio between these two quantities could be used to determine ϕ_F, however, an absolute calibration of the intensity measurements would be needed. An alternative, then, is to use the ratio between the measured quantities for the unknown sample and the reference sample, thus eliminating any calibration factor. Furthermore, the refractive index of the solution alters the maximum light that can be gathered in an emission cone, so a correction based on this effect is added an then allows one to write the equation of Brouwer's method

$$\phi_F = \phi_F^{ref} \frac{\int_{\lambda_0}^{\lambda_1} F(\lambda)d\lambda}{\int_{\lambda_0}^{\lambda_1} F_{ref}(\lambda)d\lambda} \frac{f_{ref}(\lambda)}{f(\lambda)} \frac{n^2}{n_{ref}^2}. \tag{7}$$

In this equation, all the "ref" subscripts denote the reference sample quantities. An additional correction, to account for the non-monochromatic excitation source, was added as an average of the absorbed intensity over the excitation profile $I_{ex}(\lambda)$ of the fluorimeter, redefining $f(\lambda)$ then as $f(\lambda) = \frac{\int_{\lambda_0}^{\lambda_1} I_{ex}(\lambda)\left(1 - 10^{-A(\lambda)}\right)d\lambda}{\int_{\lambda_0}^{\lambda_1} I_{ex}(\lambda)d\lambda}$. This procedure was then used for the two molecules dissolved in pure DMSO and the 50/50 DMSO/H_2O solution. Similar absorbance values of 0.2 were used for all solutions, which had concentrations of about 10^{-7} M.

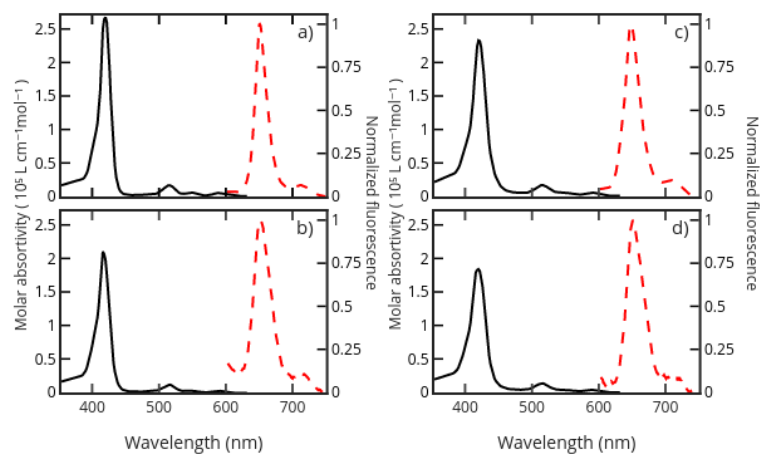## Absorption and Fluorescence spectra

Figure 11: The measured absorption spectra (solid black lines) and normalized fluorescence spectra (red dashed lines) of 3-cis-PtTPyP in DMSO (a) and in 50/50 DMSO/H_2O (b), and 4-cis-PtTPyP in DMSO (c) and in 50/50 DMSO/H_2O (d).

Source: By the author

Appendix B Time-resolved Fluorescence

In the figure 12, the experimental data were represented as a continuous curve because of the high quantity of points. The constructed confidence bands take into account a maximum error of 10% on the determination of τ_F. The curve in 12.a has a long lifetime, and it is an example of how at a short time after excitation ($< 3\ ns$), the behavior of the curve is not always well described by the model. This is a feature that is sample-dependent, and is principally caused by different relative intensities of fluorescence emission and scattered laser light. An another example is given in 12.b for the sample with $\tau_F = 0.61 \quad 0.06\ ns$. In this case, the fitting has a broader error band at times around 0.8 ns and 1.5 ns, which indicates that the τ_F value is being greatly influenced by the behavior of the curve in this range. Although the curves are often over-fitted by the model, it has already been shown that this method can produce reliable results, as in figure 3.c, in which a sample of Rhodamine B in ethanol had its fluorescence lifetime correctly determined. The fluorescence quantum yield of Rhodamine B in ethanol is around 50% in room temperature (14), so the fluorescence emission is much more intense in comparison to the studied porphyrins, with quantum yields between 0.8% and 0.07%. Also, for high quantum yields, the fluorescence emission may be way more intense than the scattered radiation. That is why the fitted curve is also well fit for times less than $2\ ns$ after excitation. Meanwhile, for low quantum yields, scattering and fluorescence emission are closer in magnitude and thus lead to the case of figure 12.a.
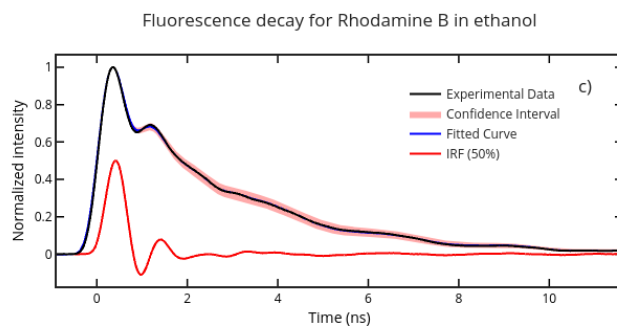

To be continued

35
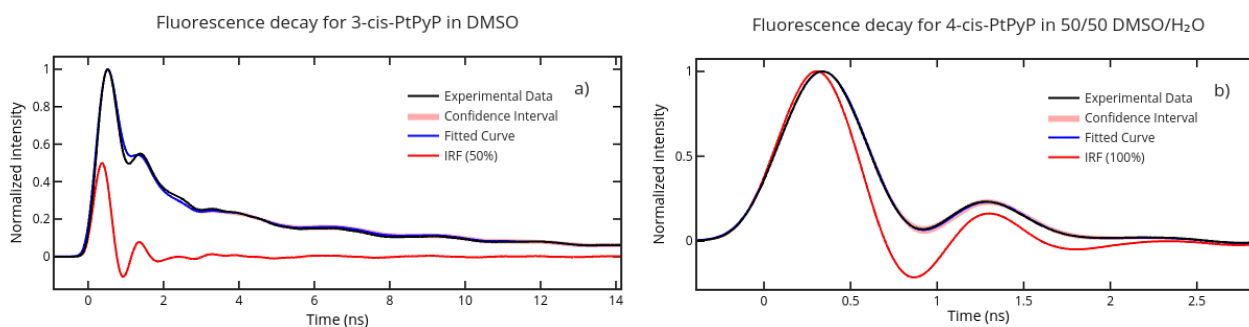
Continuation

Figure 12: Three fluorescence decay curves from different samples. The experimental curves are shown as a solid black line and the curve fitted to them as a solid blue line. The IRF in solid red lines is represented either multiplied by 50% or by its normalized value (100%). Additionaly , red confidence bands envelope the fitted curve and take into account a variation of 10% of the τ_F values.

Source: By the author

Appendix C   Visualization of the precision in the τ_{isc} values

The value of τ_{isc} determined for the 3-cis-PtTPyP molecule in DMSO was $\tau_{isc} = 14 \quad 1\ ns$. What this means graphically is more precisely shown in figure 13. Different τ_{isc} were forced into the fitting model M(a) to show how it responds graphically (σ_a is left as the only free-parameter). One can principally see the difficulty for the other values to follow the time-profile of the signal after the second excitation. Before the second excitation, the curves are all the same, as is described by eqs. (4) and (5).
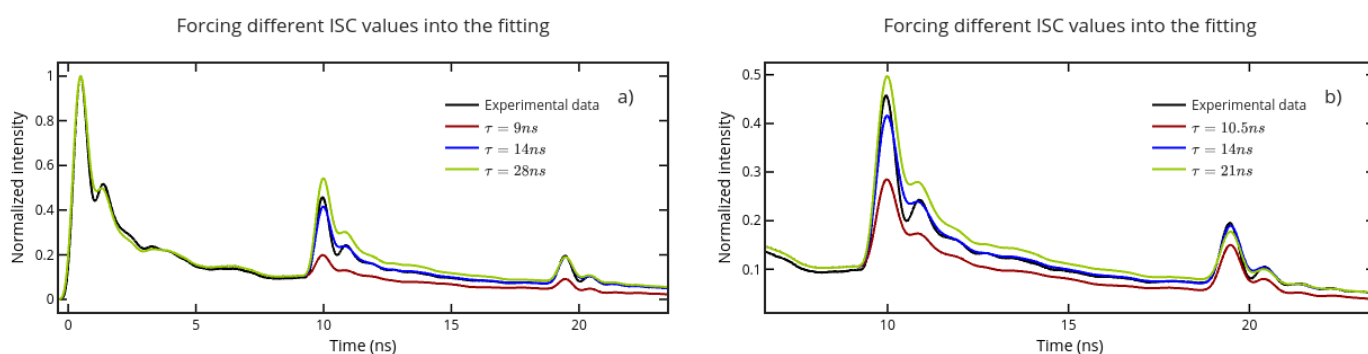

Figure 13: The figures a) and b) both show the best fitted curve with $\tau_{isc} = 14\ ns$ and also other curves which represent a minimum error of 25% in the determination of τ_{isc}. In figure b), the first pulse is left out, so the third and second pulses are better visualized.

Source: By the author

Appendix D Comparison of M(a) and M(b) models

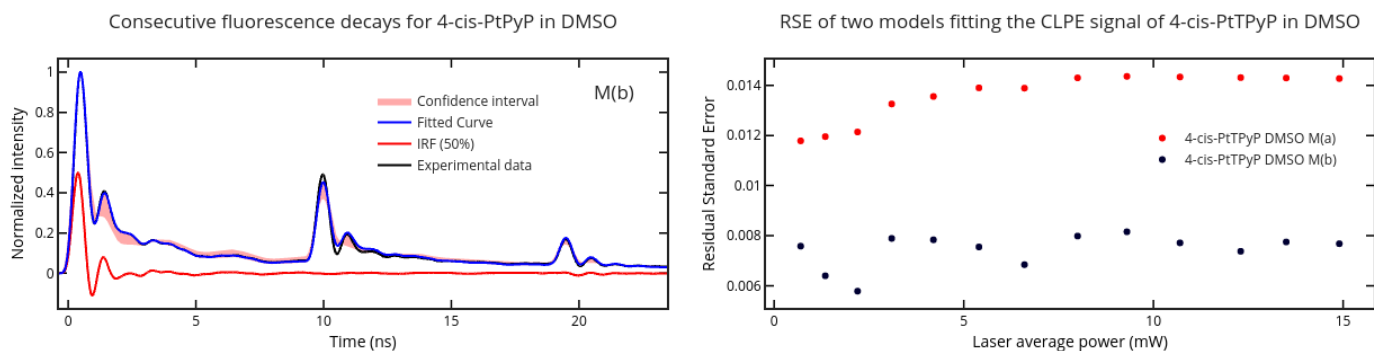Comparison of both models, as discussed in section 3.3.3.

Figure 14: On the left, the signal of 4-cis-PtTPyP in DMSO is modeled with M(b). This plot should be compared for the same situation in figure 7. On the right, the residual standard errors of the two M(a) and M(b) applied models, as a function of laser power. The RSE values are measured always with the normalized fluorescence decay curve.

Source: By the author